ACS OMEGA

http://pubs.acs.org/journal/acsodf

Article

$CoNiSe_2$ Nanostructures for Clean Energy Production

Balasubramanian Jansi Rani, Ganesan Ravi, Rathinam Yuvakkumar,* Balasubramaniam Saravanakumar, Mariyappan Thambidurai, Cuong Dang, and Dhayalan Velauthapillai*

Cite This: *ACS Omega* 2020, 5, 14702−14710

Read Online

ACCESS | Metrics & More | Article Recommendations

ABSTRACT: Comparative investigation of the electrochemical oxygen evolution reaction (OER) activity for clean energy production was performed by fabricating three different electrodes, namely, $NiSe_2$, $CoSe_2$, and $CoNiSe_2$, synthesized by hydrothermal treatment. Cubic, orthorhombic, and hexagonal structures of $NiSe_2$, $CoSe_2$, and $CoNiSe_2$ were confirmed by X-ray diffraction (XRD) and also by other characterization studies. Perfect nanospheres, combination of distorted nanospheres and tiny nanoparticles, and sharp-edge nanostructures of $NiSe_2$, $CoSe_2$, and $CoNiSe_2$ were explored by surface morphological images. Higher OER activity of the binary $CoNiSe_2$ electrode was achieved as 188 mA/g current density with a comparatively low overpotential of 234 mV along with higher conductivity and low charge transfer resistance when compared to its unary $NiSe_2$ and $CoSe_2$ electrodes. A low Tafel slope value of 82 mV/dec was also achieved for the same binary $CoNiSe_2$ electrode in a half-cell configuration. The overall 100% retention achieved for all of the fabricated electrodes in a stability test of OER activity suggested that the excellent optimum condition was obtained during the synthesis. This could definitely be a revelation in the synthesis of novel binary combinations of affordable metal selenides for clean energy production.

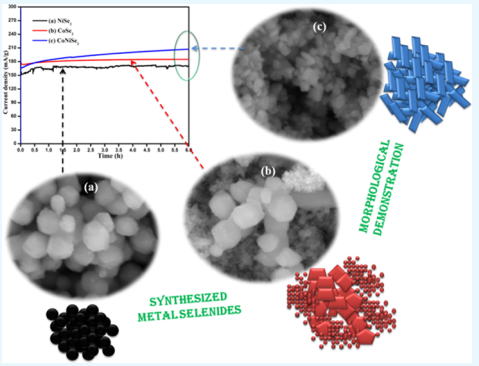

1. INTRODUCTION

In the last few decades, advances made in economic and technological developments have increased the demand for energy consumption, leading to blind utilization of fossil fuels, which has harmed the environment.[1] It is very complicated for mankind in the near future to postpone the worsening of the future generation at any cost.[2] Fossil fuels such as coal, petroleum, and natural gas are being consumed by mankind every day, and their demand has been increasing as well with time. Constant utilization of fossil fuels is leading to environmental pollution, causing global warming and changes in climatic conditions.[3] This is a serious issue, which has inspired researchers to seek for alternate energy sources using renewable energy sources as an efficient alternative to fossil fuels.[4] Renewable energy resources are green and efficient sources of energy that have an important role to play in both current and future human lives without harming the environment.[5,6] Clean energy hydrogen and oxygen can be efficiently produced using the water-splitting approach, especially the electrochemical water oxidation process for sustainable energy.[7,8] Electrochemical water splitting is a promising approach to split water with zero percent carbon emission, and this approach has been successfully meeting approximately 4% of the world's hydrogen demand.[9−11] It is a highly safe, environmentally friendly, and user-friendly approach to produce clean energy.[12,13] The major difficulty associated with water splitting is that an external energy (237 kJ/mol) needs to be supplied to drive the process due to its uphill reaction kinetics.[14]

Water splitting generally comprises the oxygen evolution reaction (OER) and the hydrogen evolution reaction (HER). These two half-reactions can be expressed as follows: HER: $2H^+ + 2e^- \rightarrow H_2$; and OER: $2H_2O \rightarrow O_2 + 4H^+ + 4e^-$.[15] The overall efficiency of water splitting depends on the electrocatalyst, which progressively leads the entire reaction to produce O_2 and H_2. Although the reactions seem quite simple, their actual kinetics are quite sluggish and thermodynamically unfavorable.[16,17] Generally, HER is a two-step electron process and OER is a four-step electron process. Hence, initiating a reaction with OER is a very slow and complicated process. Thus, electrocatalysts, which are important to produce O_2 through OER kinetics with a low overpotential, low cost, and high stability, are still of utmost importance to researchers.[18−20] Traditionally, Ru and Ir oxides have been reported as effective OER catalysts and Pt-based materials have been reported as effective HER catalysts.[21,22] Moreover, the less abundance and high cost of such catalysts are unfavorable for

Received: April 1, 2020
Accepted: May 14, 2020
Published: June 9, 2020

https://dx.doi.org/10.1021/acsomega.0c01476
ACS Omega 2020, 5, 14702−14710

large-scale applications.[23] Hence, the focus of researchers has been on earth-abundant and low-cost electrocatalysts with high efficiency, and thus transition-metal-based oxides and other derivatives have been studied and reported by many research groups.[24−26]

Among other derivatives of transition metals, selenide derivatives of Ni and Co have been found to possesses unique electrochemical catalytic activity and their material properties could be tuned by appropriately tuning their parameters and strategies.[27,28] They specifically have high stability, corrosion-resistance ability, a suitable electronic band structure and alignment, and apt valence edges for electrolyzing water.[29−33] A number of studies have investigated the catalyzing abilities of Ni and Co selenides.[34−37] Still, a full-fledged exploration of such nanostructured catalysts is not yet available. Generally, material morphology and size matter a lot in electrochemical reactions. One of the best ways to manipulate such characteristics of nanostructured selenides is the synthesis method. Many synthesis routes are being used, and among them, the hydrothermal method is the most convenient and desired one to yield products using nanostructured material processing.[38−42]

In this study, a comparative analysis of unary $NiSe_2$ and $CoSe_2$ and binary $CoNiSe_2$ nanostructures has been made and the mentioned nanostructures were optimally synthesized by employing a controlled hydrothermal route. Preliminary confirmation of the metal selenides was done by X-ray diffraction (XRD), Raman, photoluminescence (PL), and Fourier transform infrared (FTIR) studies. The nanospherical morphology of the synthesized products was confirmed by field emission scanning electron microscopy (FESEM) analysis. The comparative electrochemical OER activities of the unary $NiSe_2$ and $CoSe_2$ and the binary $CoNiSe_2$ nanostructures were extensively discussed with respect to the electrochemical mechanism with the help of cyclic voltammetry (CV), linear sweep voltammetry (LSV), electrochemical impedance spectroscopy (EIS), Tafel slope, and CA studies.

2. RESULTS AND DISCUSSION

Transition-metal selenides such as $NiSe_2$, $CoSe_2$, and $CoNiSe_2$ nanostructures were synthesized by employing the hydrothermal route. The phase and structural confirmation was made by an XRD study as shown in Figure 1a−c. Sharp, highly resolved peaks were obtained for all of the three samples, which show the formation of good crystalline nanostructures. Figure 1a exemplifies the XRD spectra of cubic $NiSe_2$ as given in JCPDS card number #89-7161. It also replicates the highly crystalline nature of the sample by the peaks corresponding to the plane values such as (200), (210), (211), (220), (311), (222), (023), (321), (400), (421), and (332) centered at 2θ values of 29.8, 33.6, 36.9, 42.7, 50.5, 53.2, 55.3, 57.9, 62.4, 72.7, and 74.6°, respectively. Figure 1b represents the XRD pattern of orthorhombic $CoSe_2$ of JCPDS card number #53-0449, whose corresponding peaks match the crystallographic planes (101), (111), (120), and (211) centered at 2θ values of 30.7, 34.6, 35.7, and 47.9°, respectively. The diffraction peaks demonstrated for $CoSe_2$ are slightly amorphous in nature, which will promote the electrochemical reaction during water oxidation. Figure 1c represents the XRD pattern of the hexagonal $CoNiSe_2$ nanostructure of JCPDS card number #65-7038 whose diffraction peaks correspond to the crystal planes (100), (101), (102), (110), and (202) centered at 2θ values of 28.4, 32.8, 44.5, 49.8, and 69.1°, respectively. All of the three samples perfectly matched with their standard ones. The crystallite sizes were calculated from the Debye−Scherer formula, which has been reported in our previous study.[45] As per the data, the calculated average crystallite sizes are 34, 29, and 32 nm, respectively. None of the impurity peaks was observed along with the characteristic diffraction peaks of $NiSe_2$, $CoSe_2$, and $CoNiSe_2$ nanostructures. Hence, the prepared unary and binary selenides were explicitly confirmed by XRD spectra.

Raman spectra of the synthesized unary and binary selenides are illustrated in Figure 2a−c, which represent the character-

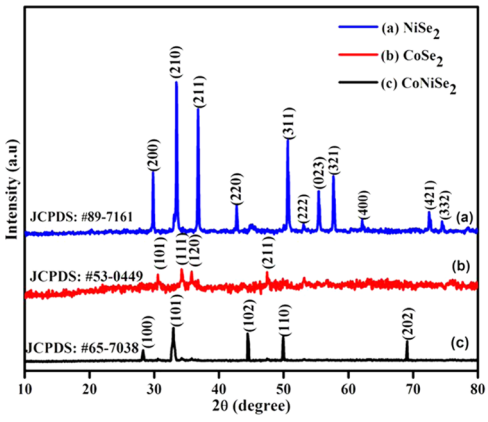

Figure 1. XRD spectra of (a) $NiSe_2$, (b) $CoSe_2$, and (c) $CoNiSe_2$ nanostructures.

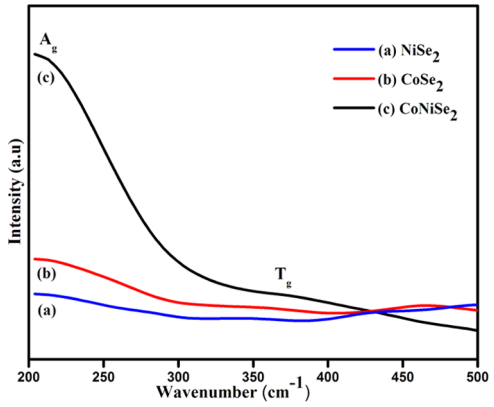

Figure 2. Raman spectra of (a) $NiSe_2$, (b) $CoSe_2$, and (c) $CoNiSe_2$ nanostructures.

istic phonon vibration modes of the prepared nanostructures. Figure 2a,b represents the two slight humplike peaks of $NiSe_2$ and $CoSe_2$ nanostructures around 210−220 and 345−355 cm^{-1}. These are the characteristic vibration modes of each unary selenide such as $NiSe_2$ and $CoSe_2$ nanostructures.[46,47] Figure 2c represents A_g and T_g phonon vibration modes of the binary $CoNiSe_2$ nanostructures at the wavenumbers 208 and 378 cm^{-1}, respectively.[48] The humplike peaks of all of the three samples represent their moderate amorphous nature, as already evidenced from XRD spectra, and also such a kind of amorphous nature will support the sustainable electrochemical reaction.

The emission nature, the presence of interstitial and oxygen vacancies present in the samples, was explicitly demonstrated

https://dx.doi.org/10.1021/acsomega.0c01476
ACS Omega 2020, 5, 14702−14710

by PL spectra as shown in Figure 3a–c. The samples were excited at 330 nm excitation wavelength. Figure 3a,b

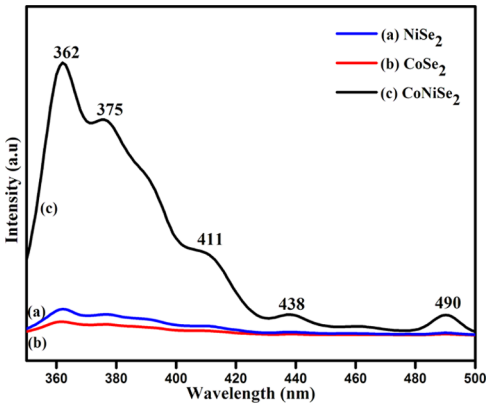

Figure 3. PL spectra of (a) $NiSe_2$, (b) $CoSe_2$, and (c) $CoNiSe_2$ nanostructures.

demonstrates the slight humplike peaks around 360 nm, which are raised due to the recombination of photogenerated electrons and holes at a lower conductance band and an upper valence band of the samples. This is called near band edge emission (NBE) of the semiconductor derivatives. Figure 3c represents the five appreciable emission peaks at 362, 375, 411, 438, and 490 nm. The peaks at 362, 375, and 411 represent the NBE emission of photogenerated charge carriers of different energy bands. The peak at 438 nm represents the characteristic d–d transition of Ni- and Co-based derivatives.[44] The peak at 490 nm represents the oxygen vacancies present in the binary $CoNiSe_2$ nanostructure, whereas the absence of an oxygen vacancy peak is observed in the unary selenides. It evidently confirms that the prepared binary nanostructure governed by oxygen vacancies undoubtedly improves the diffusion of the active material at the electrode surface during inter- and deintercalation of electrode–electrolyte ions.[49] Hence, the entire details about the emissive nature and vacancies present in the samples were extensively studied from PL spectra.

Figure 4a–c demonstrates the FTIR spectra of the prepared unary and binary metal selenides in the range 500–4000 cm^{-1}, which confirms the characteristic vibrations and functional groups present in the samples. The deep absorption band observed around 3300–3400 and 1500–1600 cm^{-1} could be

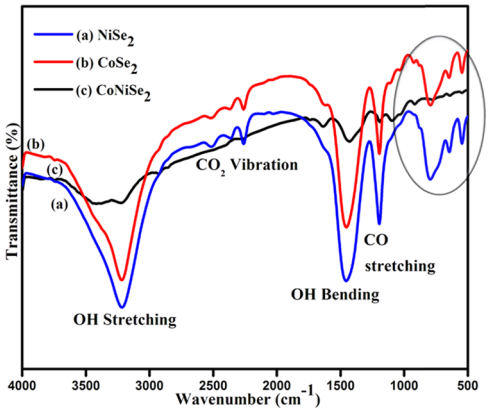

Figure 4. FTIR spectra of (a) $NiSe_2$, (b) $CoSe_2$, and (c) $CoNiSe_2$ nanostructures.

attributed to the OH stretching and bending vibrations of water molecules adsorbed at the surface of the samples from atmospheric moisture.[6] The bands observed from 2200 to 2400 cm^{-1} could be attributed to the CO_2 vibration of the samples. The band at 1100–1200 cm^{-1} could be attributed to CO stretching vibration.[6] The bands observed from 500 to 900 cm^{-1} could be attributed to the mere characteristic vibration modes of the prepared samples. These bands confirm the Ni and Co complex bonding with Se at the same time as already reported in the literature.[50,51] The suppression in band intensity observed for the binary $CoNiSe_2$ nanostructures might be due to the multiple vibration modes of Ni and Co with Se in diverse frequencies. Hence, FTIR confirmed the formation of unary $NiSe_2$ and $CoSe_2$ and binary $CoNiSe_2$ nanostructures.

Figure 5a–f shows the surface morphologies of the prepared nanostructures at two different scale ranges of 2 μm and 500 nm. Figure 5a,d shows the typical nanospherical morphologies of the prepared unary $NiSe_2$ nanostructures with uniform shapes and sizes. Generally, low agglomeration associated with the nanostructures strongly evidences the optimum control of growth parameters during synthesis. Low agglomeration usually increases the possibility of obtaining active sites at the surface during the electrochemical reaction.[52] In addition, easy migration of the active material from the surface and its return back is more possible in this case, which could help improve the electrochemical OER activity for clean energy production. Each nanosphere size approximately ranges from 100 to 150 nm with an edgeless outer surface having a typical spherical nature, which evidences the high surface-to-volume ratio of the material. Figure 5b,e shows the surface morphologies of $CoSe_2$ nanostructures at 2 μm and 500 nm, respectively. These images reveal the formation of two different morphologies of distorted nanospheres and tiny nanoparticles of $CoSe_2$. Distorted nanospheres with some edges having a particle size around 100–120 nm and tiny nanoparticles of sizes approximately 30–80 nm were observed. These kinds of combined morphologies of nanostructures could also support the electrochemical reaction by promoting more active sites available at the electrode surface. Figure 5c,f shows the surface morphology of binary $CoNiSe_2$ nanostructures at 2 μm and 500 nm, respectively. These images show the sharp-edge undefined shape particle formation of approximate particle size ranges from 80 to 120 nm with some agglomeration. This kind of agglomeration observed during nanoparticle formation in binary metal selenide nanostructures might be due to the number of magnetic particle association during nucleation to form hexagonal $CoNiSe_2$ nanostructures. Also, the sharp-edge particles having a smaller particle range could improve the participation of active sites in more numbers in the reaction, which helped promote conductivity and OER activity. Moreover, the SEM images confirmed the particle growth mechanism of unary and binary metal selenides in the controlled optimized condition of hydrothermal treatment in this work.

Figure 6a–c shows the cyclic voltammogram study of the prepared electrodes in a 1 M alkaline medium in a half-electrochemical cell design at different scan rates such as 10, 30, 50, 80, and 100 mV/s to estimate the electrochemical oxidation and reduction nature. From Figure 6a–c, the perfect redox (reduction/oxidation) behavior of the fabricated electrodes with good current density values can be visibly observed. Oxidation and reduction potentials are also estimated from the

https://dx.doi.org/10.1021/acsomega.0c01476
ACS Omega 2020, 5, 14702–14710

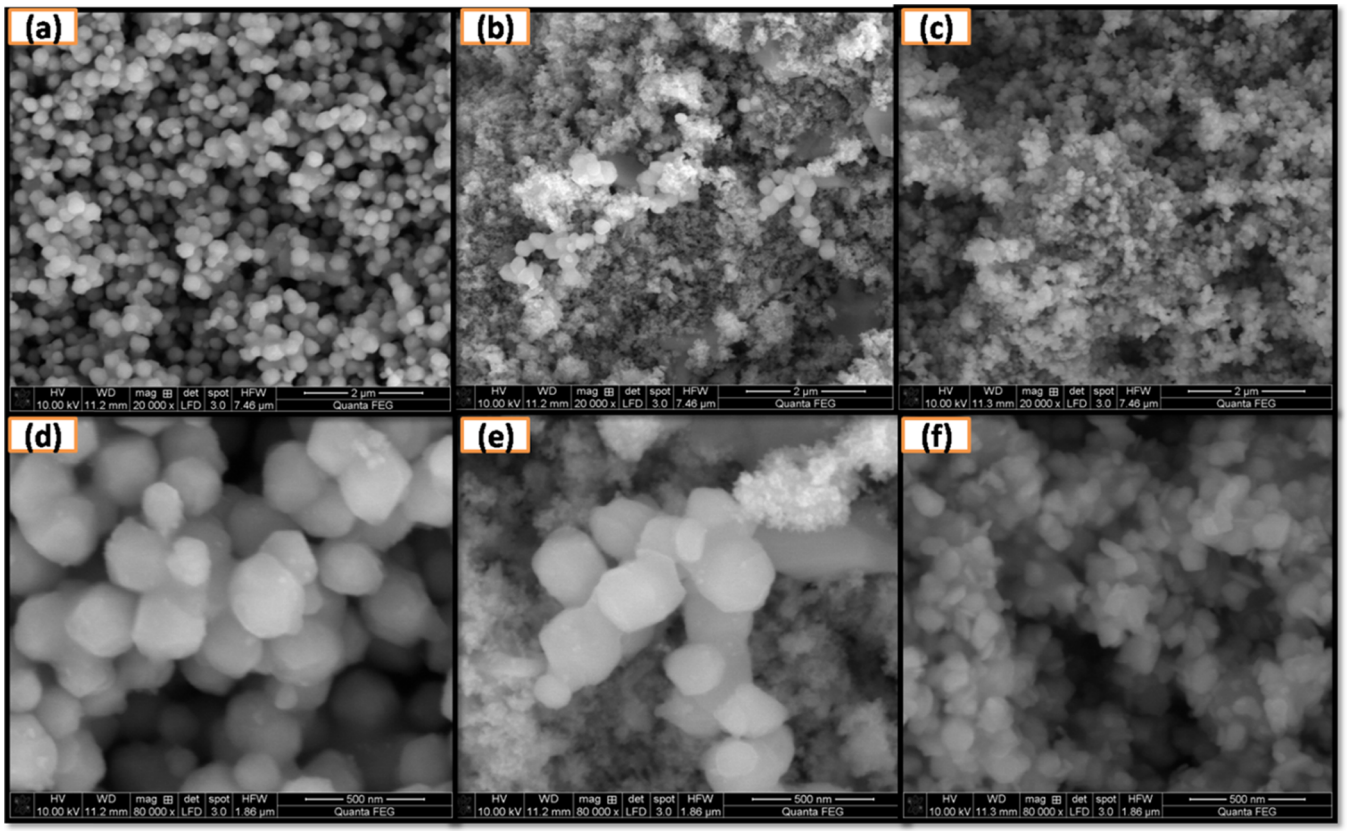

Figure 5. SEM images of (a, d) $NiSe_2$ nanostructures at 2 μm and 500 nm, (b, e) $CoSe_2$ nanostructures at 2 μm and 500 nm, and (c, f) $CoNiSe_2$ nanostructures at 2 μm and 500 nm.

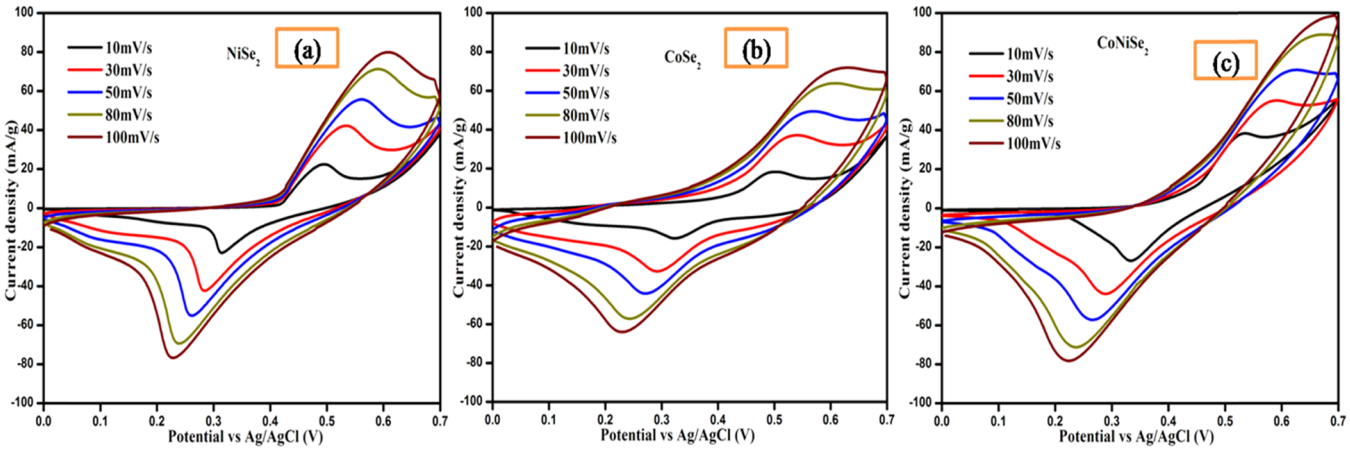

Figure 6. CV graphs of (a) $NiSe_2$, (b) $CoSe_2$, and (c) $CoNiSe_2$ nanostructured electrodes in a conventional half-cell design at different scan rates of 10, 30, 50, 80, and 100 mV/s in 1 M KOH.

CV curves for different unary and binary metal selenides prepared in this work. Hence, binary $CoNiSe_2$ nanostructured electrodes exhibited a higher density for the same fixed given potential window from 0 to 0.7 V when compared to the other prepared unary metal selenides. Moreover, the specific capacitance was calculated from the conventional formula $C = \frac{\int_{V_1}^{V_2} I(V)\mathrm{d}V}{(V_2 - V_1)Sm}$, where $I(V)\mathrm{d}V$ is the area of the CV curve, m refers to the mass of the active material loaded on the Ni foam substrate, S refers to the scan rate value, and $(V_2 - V_1)$ refers to the potential window difference. As per the formula, the calculated specific capacitance values at 10 mV/s scan rate are 437, 508, and 581 F/g for $NiSe_2$, $CoSe_2$, and $CoNiSe_2$, respectively. It clearly denotes that the binary $CoNiSe_2$ electrode exposed a comparatively higher specific capacitance than the others, which might be due to the combined effect of multiple valence states of Co and Ni redox states as $CoNiSe_2$ nanostructures. Subsequently, at a given potential, Ni (Ni^{2+}/Ni^{3+}) and Co (Co^{2+}/Co^{3+}) underwent the redox reaction simultaneously and released more electrons to the circuit, causing higher current density and CV area. From this, the fabricated $CoNiSe_2$ binary electrode is expected to oxidize water for producing clean energy in an efficient way compared to unary electrodes.

https://dx.doi.org/10.1021/acsomega.0c01476
ACS Omega 2020, 5, 14702−14710

The water oxidation behavior of the fabricated electrodes was investigated by an LSV curve run at a 10 mV/s scan rate at a fixed potential range from −0.2 to 1.0 V vs Ag/AgCl, which could be a better optimum potential for the OER activity of semiconductor electrodes. Figure 7a−c shows the typically

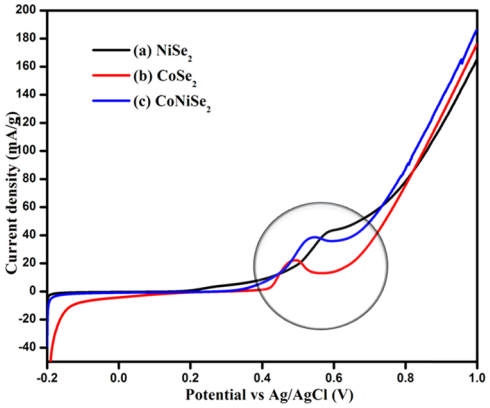

Figure 7. LSV curves of (a) $NiSe_2$, (b) $CoSe_2$, and (c) $CoNiSe_2$ nanostructured electrodes in a conventional half-cell design at a 10 mV/s scan rate in 1 M KOH.

defined oxidation curves of the fabricated electrodes $NiSe_2$, $CoSe_2$, and $CoNiSe_2$, respectively, as 159, 176, and 188 mA/g. It clearly shows that a comparatively higher current density can be observed for the fabricated binary metal $CoNiSe_2$ nanostructures. The variation in current density is less among the fabricated unary and binary metal selenide electrodes even though the overpotential varied appreciably. In the case of OER activity, the overpotential is considered as a more important phenomenon than the current density due to its driving capability of the entire water oxidation reaction. The estimated overpotential values are 297, 278, and 234 mV, respectively, for $NiSe_2$, $CoSe_2$, and $CoNiSe_2$ nanostructured electrodes. Hence, the comparatively lower overpotential and the higher current density obtained by the $CoNiSe_2$ electrode might be due to the combined possible phenomena such as (a) multiple oxidation states of $CoNiSe_2$ compared to its unary metal selenides; (b) favorable sharp-edge morphology of the $CoNiSe_2$ electrode in the nanoscale range, which is responsible for the easy capture of electrolyte ions during the reaction and also more active particles benefitted at the electrode/electrolyte interface; and (c) the vacancies present in the binary metal selenide nanostructures, which are undoubtedly responsible for the sustainable and rapid OER kinetics and also the higher conductivity. These features synergistically favor the OER activity of the $CoNiSe_2$ electrode to produce clean energy. At the outset, when a potential is applied to the system, the oxidation of active elements (Ni: Ni^{2+}/Ni^{3+} and Co: Co^{2+}/Co^{3+}) takes place at the outer layer of the electrode. The oxidized state of Ni^{3+} and Co^{3+} continuously produces M(Ni/Co)−OOH species, which are the active participants of OER activity in alkaline electrolyte solution.[53−55] The products $NiSe_2$ and $CoSe_2$ exist under the oxidative layer maintaining the electrical conductivity, which further supports the electrocatalytic activity.

In addition, the formation of binary $CoNiSe_2$ nanostructures is again confirmed by the oxidation potential afforded by the electrode. Cleary, the oxidation potential values of $NiSe_2$, $CoSe_2$, and $CoNiSe_2$ nanostructured electrodes are 0.57, 0.48, and 0.53 V vs Ag/AgCl, respectively. It clearly evidenced that the binary selenide $CoNiSe_2$ oxidized at the potential falls between the oxidation potentials of its unary. On the whole, the binary $CoNiSe_2$ nanostructured electrode is a much better candidate regarding current density and overpotential evidenced by the LSV spectra.

The Nyquist plot of EIS spectra of the fabricated electrodes in 1 M KOH is given in Figure 8a. Charge transportation and reaction kinetics of the electrodes are in the fixed frequency range from 100 kHz to 100 MHz. The graph explores two regions, namely, semicircle arc and spike, which represent the charge transfer resistance offered by the electrodes and the conductivity afforded by the electrodes, respectively. As per the graph, the estimated charge transfer resistances of $NiSe_2$, $CoSe_2$, and $CoNiSe_2$ nanostructured electrodes are 101, 80, and 48 Ω, respectively. It clearly confirms that a comparatively lower charge transfer resistance is offered by the binary $CoNiSe_2$ electrode than its unary one and also has a higher conductivity, which might be due to the multiple oxidation of Co and Ni during the electrochemical reaction, which released more electrons to the circuit than its binary one. This feature could also combine sharp-edge morphology, oxygen vacancy, and multiple oxidations. It strongly supports the results

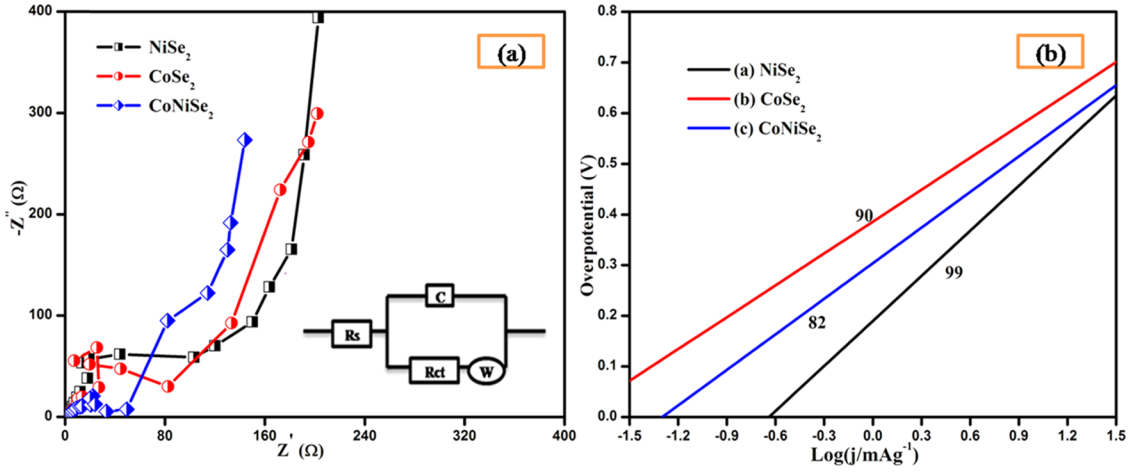

Figure 8. (a) EIS spectra in the 100 kHz to 100 MHz frequency range. (b) Tafel slopes of $NiSe_2$, $CoSe_2$, and $CoNiSe_2$ nanostructured electrodes in a conventional half-cell design in 1 M KOH.

https://dx.doi.org/10.1021/acsomega.0c01476
ACS Omega 2020, 5, 14702−14710

obtained from CV and LSV. It can also be correlated from the Tafel plot of the fabricated electrodes in Figure 8b.

The Tafel slope revealed the inherent rate-limiting step of the candidate. The linear part of the Tafel slope gives the Tafel slope value of the fabricated electrodes, which is drawn from the equation $\eta = b\ \log(j) + a$, where η is the overpotential, b is the Tafel slope, and j is the current density. From the investigation, the obtained Tafel slope values of $NiSe_2$, $CoSe_2$, and $CoNiSe_2$ nanostructured electrodes were found to be 99, 90, and 82 mV/dec, respectively. It is clear that the unary electrodes possess a higher Tafel slope value, which means that they required more driving potential to establish 10 mA current and it also indicated the rate-determining process of the second electron. Moreover, the result markedly proved that the binary $CoNiSe_2$ nanostructures possess 82 mV/dec, which falls under the first rate-limiting step of the electrons, which might be due to the better electronic conductivity of the binary metal selenide due to its oriented chemical coupling of Co and Ni with Se. During the reaction, the electrochemical kinetics involved in Ni- and Co-based selenides could be the reaction of OH^- radicals with an adsorbed O atom to produce OOH species ($Ni/Co-O + OH^- \rightarrow Ni/Co-OOH + e^-$), along with the pre-equilibrium steps of $NiSe_2$ and $CoSe_2$ such as $Ni-OH + OH^- \rightarrow Ni-O + e^- + H_2O$ or $Ni-OH \rightarrow Ni-O + H^+ + e^-$ and $2Co-O + H_2O \rightarrow Co-OOH + Co-OH$, respectively.[56,57] Hence, the Tafel slope of the electrodes proves that the remarkable activity of the fabricated binary $CoNiSe_2$ nanostructured electrode could also be due to its excellent electronic conductivity compared to the unary electrodes.

Electrochemical stability of the fabricated electrodes was tested by a CA study for 6 h beneath the prolonged OER activity as shown in Figure 9a–c. From the CA graph, it can be

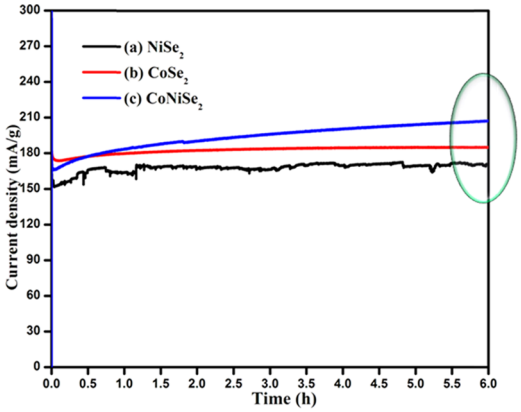

Figure 9. CA studies of (a) $NiSe_2$, (b) $CoSe_2$, and (c) $CoNiSe_2$ nanostructured electrodes in a conventional half-cell design for 6 h.

clearly seen that the three electrodes exhibited excellent electrochemical stability over 6 h with 100% retention of its initial capacity, which might be due to the lack of degradation in its structure and robustness. During the entire reaction, the fabricated electrodes $NiSe_2$, $CoSe_2$, and $CoNiSe_2$ exhibited 170, 186, and 207 mA/g, respectively. It explains the higher OER activity observed for the binary $CoNiSe_2$ electrode. This kind of linear ramp in current density suggested the excellent mass diffusion and mechanical robustness of the electrodes. Moreover, the slight disturbance that occurred in the case of unary ($NiSe_2$ and $CoSe_2$) metal selenides when compared to its binary one might be due to the continuous electrochemical OER activity, which may disturb the particle nature that gradually occurs during electrochemical milling.[48] $CoNiSe_2$ could overcome it owing to its robust nature and surface morphology. Table 1 shows the comparative analysis of the overpotential value afforded by our best performing electrode with the literature.

Table 1. Comparative Analysis of the Obtained Best Performing Electrode Overpotential with the Literature

electrode	electrolyte	overpotential (mV)	references
$CeO_2/CoSe_2$	0.1 M KOH	288	51
$CoSe_2$	1 M KOH	430	53
$NiSe_2$	1 M KOH	250	53
$CoNiSe_2$	1 M KOH	307	54
$CoSe_2$	0.1 M KOH	320	55
$CoNiSe_2$@Ni foam	1 M KOH	234	present work

In this work, earth-abundant metal-based unary and binary selenides such as $NiSe_2$, $CoSe_2$, and $CoNiSe_2$ nanostructures were synthesized via the hydrothermal route. Preliminary characterizations such as XRD, Raman, PL, and FTIR were performed. Surface morphological analysis was explored from SEM images such as nanospheres, distorted nanospheres, and sharp-edge undefined nanostructures for $NiSe_2$, $CoSe_2$, and $CoNiSe_2$ nanostructures, respectively. The electrochemical OER activity of each metal selenide was investigated in a half-cell configuration, and experiments such as CV, LSV, EIS, and CA were performed. From the results, binary metal selenide $CoNiSe_2$ was found to have performed well, which proved to be an efficient material with a low overpotential for electrochemical clean energy production. Further, binary metal selenides with novel nanoarchitectures with graphene-based composite materials were found to have a great impact on their catalytic activity; besides, the higher conductivity of such composites would be expected to lower their overpotential for real-time large-scale applications in future works. Hence, the electrochemical investigations clearly showed that the binary metal selenide nanostructured electrode could be used for sustainable OER activity to produce clean energy. This kind of binary metal derivative synthesis could be of great potential for researchers working in energy conversion and clean energy production fields.

3. CONCLUSIONS

Three different metal selenides, namely, $NiSe_2$, $CoSe_2$, and $CoNiSe_2$ nanostructures, were synthesized using the hydrothermal method. Electrode fabrication was performed using each selenide on a Ni foam substrate to investigate the electrochemical property for clean energy production application. Higher current density and specific capacitance of 188 mA/g and 581 F/g, respectively, were achieved for the binary $CoNiSe_2$ electrode at 10 mV/s with a low overpotential of 234 mV. Excellent electrochemical stability was also achieved for all of the fabricated electrodes. This work could be of great help to researchers working in the energy sector for producing clean energy in a cost-effective and greener way.

4. EXPERIMENTAL SECTION

Analytical-grade nickel(II) nitrate hexahydrate ($Ni(NO_3)_2 \cdot 6H_2O$), cobalt(II) nitrate hexahydrate ($Co(NO_3)_2 \cdot 6H_2O$), and selenium powder (Se) were purchased from Sigma-Aldrich and used as received. Initially, 0.05 M selenium powder was

https://dx.doi.org/10.1021/acsomega.0c01476
ACS Omega 2020, 5, 14702−14710

dissolved in 20 mL of hydrazine hydrate. Then, 0.1 M $Ni(NO_3)_2·6H_2O$ was dissolved in 50 mL of deionized water. Then, the selenium powder solution was poured into the mixed solution dropwise under the same stirring condition. A black precipitate was formed on completion of the reaction. The same procedure was followed for $CoSe_2$ synthesis, where 0.1 M $Co(NO_3)_2·6H_2O$ was dissolved in 50 mL of deionized water and the other procedures were the same as above. To synthesize $CoNiSe_2$ nanostructures, 0.1 M $Ni(NO_3)_2·6H_2O$ and $Co(NO_3)_2·6H_2O$ were dissolved in 50 mL of deionized water and then 0.1 M selenium powder was dissolved in 20 mL of hydrazine hydrate, which was poured into the above mixture, thereby obtaining a black precipitate. These three precipitated solutions underwent homogeneous stirring of about 540 rpm for 2 h continuously; then, they were transferred into a 100 mL autoclave and subjected to a furnace for 24 h at 180 °C. After cooling back down to room temperature separately five times and dried at 80 °C in a hot-air oven. The final products were named NS_1 ($NiSe_2$), NS_2 ($CoSe_2$), and NS_3 ($CoNiSe_2$), respectively. All of the characterizations and confirmation of the samples were made using the instruments discussed in our previous study.[43] Electrochemical OER activity of the electrodes for clean energy production was performed using the Biologic SP 150 work station. Electrode preparation was also the same as that in our previous study.[44] The mass loading of each metal selenide active material synthesized in this work is 3 mg on a Ni foam substrate.

AUTHOR INFORMATION

Corresponding Authors

Rathinam Yuvakkumar − *Nanomaterials Laboratory, Department of Physics, Alagappa University, Karaikudi 630003, Tamil Nadu, India;* orcid.org/0000-0001-6779-3453; Email: yuvakkumarr@alagappauniversity.ac.in

Dhayalan Velauthapillai − *Faculty of Engineering and Science, Western Norway University of Applied Sciences, Bergen 5063, Norway*; Email: dhayalan.Velauthapillai@hvl.no

Authors

Balasubramanian Jansi Rani − *Nanomaterials Laboratory, Department of Physics, Alagappa University, Karaikudi 630003, Tamil Nadu, India*

Ganesan Ravi − *Nanomaterials Laboratory, Department of Physics, Alagappa University, Karaikudi 630003, Tamil Nadu, India*

Balasubramaniam Saravanakumar − *Laboratory for Advanced Research in Polymeric Materials (LARPM), Central Institute of Plastics Engineering & Technology (CIPET), Bhubaneswar 751024, India*

Mariyappan Thambidurai − *Centre for OptoElectronics and Biophotonics (COEB), School of Electrical and Electronic Engineering, The Photonics Institute (TPI), Nanyang Technological University, Singapore 639798;* orcid.org/0000-0001-8008-4272

Cuong Dang − *Centre for OptoElectronics and Biophotonics (COEB), School of Electrical and Electronic Engineering, The Photonics Institute (TPI), Nanyang Technological University, Singapore 639798*

Complete contact information is available at: https://pubs.acs.org/10.1021/acsomega.0c01476

Notes

The authors declare no competing financial interest.

ACKNOWLEDGMENTS

This work was supported by UGC Start-Up Research grant no. F.30-326/2016 (BSR). This work was supported by the RUSA—Phase 2 grant sanction and UGC-SAP, DST-FIST, and DST-PURSE grants. Thanks to Open Access Funding (OA-fond) (oa-fond@hvl.no) at Western Norway University of Applied Sciences, Norway.

REFERENCES

(1) Gopi, C. V. V. M.; Reddy, A. E.; Kim, H.-J. Wearable superhigh energy density supercapacitors using a hierarchical ternary metal selenide composite of $CoNiSe_2$ microspheres decorated with $CoFe_2Se_4$ nanorods. *J. Mater. Chem. A* **2018**, *6*, 7439−7448.

(2) Hua, Y.; Li, X.; Chen, C.; Pang, H. Cobalt based metal-organic frameworks and their derivatives for electrochemical energy conversion and storage. *Chem. Eng. J.* **2019**, *370*, 37−59.

(3) Wang, J.-Y.; Ouyang, T.; Li, N.; Ma, T.; Liu, Z.-Q. S, N co-doped carbon nanotube-encapsulated core-shelled CoS_2@Co nanoparticles: efficient and stable bifunctional catalysts for overall water splitting. *Sci. Bull.* **2018**, *63*, 1130−1140.

(4) Cao, L.-M.; Lu, D.; Zhong, D.-C.; Lu, T.-B. Prussian blue analogues and their derived nanomaterials for electrocatalytic water splitting. *Coord. Chem. Rev.* **2020**, *407*, No. 213156.

(5) Rani, B. J.; Ravi, G.; Yuvakkumar, R.; Ravichandran, S.; Ameen, F.; Al-Sabri, A. Efficient, highly stable Zn-doped NiO nanocluster electrocatalysts for electrochemical water splitting applications. *J. Sol-Gel Sci. Technol.* **2019**, *89*, 500−510.

(6) Rani, B. J.; Raj, S. P.; Saravanakumar, B.; Ravi, G.; Ganesh, V.; Ravichandran, S.; Yuvakkumar, R. Controlled synthesis and electrochemical properties of Ag-doped Co_3O_4 nanorods. *Int. J. Hydrogen Energy* **2017**, *42*, 29666−29671.

(7) Shi, X.; Wang, H.; Ji, S.; Linkov, V.; Liu, F.; Wang, R. $CoNiSe_2$ nanorods directly grown on Ni foam as advanced cathodes for asymmetric supercapacitors. *Chem. Eng. J.* **2019**, *364*, 320−327.

(8) Tian, L.; Wang, K.; Wo, H.; Pang, X.; Zhai, X.; Zhuang, W.; Li, T.; Chen, Y. Bundle-shaped cobalt−nickel selenides as advanced electrocatalysts for water oxidation. *Int. J. Hydrogen Energy* **2019**, *44*, 2868−2876.

(9) Moore, J. Thermal Hydrogen: An emissions free hydrocarbon economy. *Int. J. Hydrogen Energy* **2017**, *42*, 12047−12063.

(10) Najafpour, M. M.; Renger, G.; Hołyńska, M.; Moghaddam, A. N.; Aro, E.-M.; Carpentier, R.; Nishihara, H.; Eaton-Rye, J. J.; Shen, J.-R.; Allakhverdiev, S. I. Manganese compounds as water-oxidizing catalysts: from the natural water-oxidizing complex to nanosized manganese oxide structures. *Chem. Rev.* **2016**, *116*, 2886−2936.

(11) Edwards, P. P.; Kuznetsov, V. L.; David, W. I. F.; Brandon, N. P. Hydrogen and fuel cells: towards a sustainable energy future. *Energy Policy* **2008**, *36*, 4356−4362.

(12) Yang, Y.; Zhang, K.; Lin, H.; Li, X.; Chan, H. C.; Yang, L.; Gao, Q. MoS_2−Ni_3S_2 heteronanorods as efficient and stable bifunctional electrocatalysts for overall water splitting. *ACS Catal.* **2017**, *7*, 2357−2366.

(13) Wang, J.; Cui, W.; Liu, Q.; Xing, Z.; Asiri, A. M.; Sun, X. Recent progress in cobalt-based heterogeneous catalysts for electrochemical water splitting. *Adv. Mater.* **2016**, *28*, 215−230.

(14) Ming, F.; Liang, H.; Shi, H.; Mei, G.; Xu, X.; Wang, Z. Hierarchical $(Ni,Co)Se_2$/carbon hollow rhombic dodecahedra derived from metal-organic frameworks for efficient water-splitting electrocatalysis. *Electrochim. Acta* **2017**, *250*, 167−173.

(15) Lewis, N. S.; Nocera, D. G. Powering the planet: Chemical challenges in solar energy utilization. *Proc. Natl. Acad. Sci. U.S.A.* **2006**, *103*, 15729−15735.

(16) Liu, T.; Asiri, A. M.; Sun, X. Electrodeposited Co-doped $NiSe_2$ nanoparticles film: a good electrocatalyst for efficient water splitting. *Nanoscale* **2016**, *8*, 3911−3915.

(17) Cook, T. R.; Dogutan, D. K.; Reece, S. Y.; Surendranath, Y.; Teets, T. S.; Nocera, D. G. Solar energy supply and storage for the legacy and nonlegacy worlds. *Chem. Rev.* **2010**, *110*, 6474−6502.
(18) Guo, Y.; Park, T.; Yi, J. W.; Henzie, J.; Kim, J.; Wang, Z.; Jiang, B.; Bando, Y.; Sugahara, Y.; Tang, J.; Yamauchi, Y. Nanoarchitectonics for Transition-Metal-Sulfide-Based Electrocatalysts for Water Splitting. *Adv. Mater.* **2019**, *31*, No. 1807134.
(19) Morales-Guio, C. G.; Stern, L.-A.; Hu, X. Nanostructured hydrotreating catalysts for electrochemical hydrogen evolution. *Chem. Soc. Rev.* **2014**, *43*, 6555−6569.
(20) Bockris, J. O. M. Hydrogen no longer a high cost solution to global warming: new ideas. *Int. J. Hydrogen Energy* **2008**, *33*, 2129−2131.
(21) Jiao, Y.; Zheng, Y.; Jaroniec, M.; Qiao, S. Z. Design of electrocatalysts for oxygen-and hydrogen-involving energy conversion reactions. *Chem. Soc. Rev.* **2015**, *44*, 2060−2086.
(22) Hong, W. T.; Risch, M.; Stoerzinger, K. A.; Grimaud, A.; Suntivich, J.; Shao-Horn, Y. Toward the rational design of non-precious transition metal oxides for oxygen electrocatalysis. *Energy Environ. Sci.* **2015**, *8*, 1404−1427.
(23) Majhi, K. C.; Karfa, P.; Madhuri, R. Bimetallic transition metal chalcogenide nanowire array: An effective catalyst for overall water splitting. *Electrochim. Acta* **2019**, *318*, 901−912.
(24) Zou, X.; Liu, Y.; Li, G.-D.; Wu, Y.; Liu, D.-P.; Li, W.; Li, H.-W.; Wang, D.; Zhang, Y.; Zou, X. Ultrafast Formation of Amorphous Bimetallic Hydroxide Films on 3D Conductive Sulfide Nanoarrays for Large-Current-Density Oxygen Evolution Electrocatalysis. *Adv. Mater.* **2017**, *29*, No. 1700404.
(25) Xing, Z.; Liu, Q.; Asiri, A. M.; Sun, X. Closely interconnected network of molybdenum phosphide nanoparticles: a highly efficient electrocatalyst for generating hydrogen from water. *Adv. Mater.* **2014**, *26*, 5702−5707.
(26) Zhang, W.; Zhang, H.; Luo, R.; Zhang, M.; Yan, X.; Sun, X.; Shen, J.; Han, W.; Wang, L.; Li, J. Prussian blue analogues-derived bimetallic iron-cobalt selenides for efficient overall water splitting. *J. Colloid Interface Sci.* **2019**, *548*, 48−55.
(27) Lim, W. Y.; Lim, Y. F.; Ho, G. W. Pseudomorphic-phase transformation of NiCo based ternary hierarchical 2D-1D nanostructures for enhanced electrocatalysis. *J. Mater. Chem. A* **2017**, *5*, 919−924.
(28) Ma, L.; Zhou, B.; Tang, L.; Guo, J.; Liu, Q.; Zhang, X. Template confined synthesis of NiCo Prussian blue analogue bricks constructed nanowalls as efficient bifunctional electrocatalyst for splitting water. *Electrochim. Acta* **2019**, *318*, 333−341.
(29) Sobhani, A.; Salavati-Niasari, M. Cobalt selenide nanostructures: Hydrothermal synthesis, considering the magnetic property and effect of the different synthesis conditions. *J. Mol. Liq.* **2016**, *219*, 1089−1094.
(30) Kong, D.; Cha, J. J.; Wang, H.; Lee, H. R.; Cui, Y. First-row transition metal dichalcogenide catalysts for hydrogen evolution reaction. *Energy Environ. Sci.* **2013**, *6*, 3553−3558.
(31) Ganesan, P.; Sivanantham, A.; Shanmugam, S. Inexpensive electrochemical synthesis of nickel iron sulphides on nickel foam: super active and ultra-durable electrocatalysts for alkaline electrolyte membrane water electrolysis. *J. Mater. Chem. A* **2016**, *4*, 16394−16402.
(32) Chen, T.; Li, S.; Wen, J.; Gui, P.; Guo, Y.; Guan, C.; Liu, J.; Fang, G. Rational construction of hollow core-branch $CoSe_2$ nanoarrays for high-performance asymmetric supercapacitor and efficient oxygen evolution. *Small* **2018**, *14*, No. 1700979.
(33) Shang, X.; Chi, J.-Q.; Lu, S.-S.; Dong, B.; Li, X.; Liu, Y.-R.; Yan, K.-L.; Gao, W.-K.; Chai, Y.-M.; Liu, C.-G. Novel Co_xS_y/WS_2 nanosheets supported on carbon cloth as efficient electrocatalyst for hydrogen evolution reaction. *Int. J. Hydrogen Energy* **2017**, *42*, 4165−4173.
(34) Chi, J.-Q.; Yan, K.-L.; Xiao, Z.; Dong, B.; Shang, X.; Gao, W.-K.; Li, X.; Chai, Y.-M.; Liu, C.-G. Trimetallic NiFeCo selenides nanoparticles supported on carbon fiber cloth as efficient electrocatalyst for oxygen evolution reaction. *Int. J. Hydrogen Energy* **2017**, *42*, 20599−20607.
(35) Lan, K.; Li, J.; Zhu, Y.; Gong, L.; Li, F.; Jiang, P.; Niu, F.; Li, R. Morphology engineering of $CoSe_2$ as efficient electrocatalyst for water splitting. *J. Colloid Interface Sci.* **2019**, *539*, 646−653.
(36) Hussain, R. A.; Hussain, I. Fabrication and applications of nickel selenide. *J. Solid State Chem.* **2019**, *277*, 316−328.
(37) Ansari, F.; Sobhani, A.; Salavati-Niasari, M. Sol−gel auto-combustion synthesis of $PbFe_{12}O_{19}$ using maltose as a novel reductant. *RSC Adv.* **2014**, *4*, 63946−63950.
(38) Liu, Y.; Hua, X.; Xiao, C.; Zhou, T.; Huang, P.; Guo, Z.; Pan, B.; Xie, Y. Heterogeneous spin states in ultrathin nanosheets induce subtle lattice distortion to trigger efficient hydrogen evolution. *J. Am. Chem. Soc.* **2016**, *138*, 5087−5092.
(39) Wang, F.; Li, Y.; Shifa, T. A.; Liu, K.; Wang, F.; Wang, Z.; Xu, P.; Wang, Q.; He, J. Selenium-enriched nickel selenide nanosheets as a robust electrocatalyst for hydrogen generation. *Angew. Chem., Int. Ed.* **2016**, *55*, 6919−6924.
(40) Swesi, A. T.; Masud, J.; Liyanage, W. P. R.; Umapathi, S.; Bohannan, E.; Medvedeva, J.; Nath, M. Textured $NiSe_2$ film: bifunctional electrocatalyst for full water splitting at remarkably low overpotential with high energy efficiency. *Sci. Rep.* **2017**, *7*, No. 2401.
(41) Jansi Rani, B.; Mageswari, R.; Ravi, G.; Ganesh, V.; Yuvakkumar, R. Design, Fabrication, and Characterization of Hematite (α-Fe_2O_3) Nanostructures. *JOM* **2017**, *69*, 2508−2514.
(42) Li, W.-N.; Yuan, J.; Shen, X.-F.; Gomez-Mower, S.; Xu, L.-P.; Sithambaram, S.; Aindow, M.; Suib, S. L. Hydrothermal synthesis of structure-and shape-controlled manganese oxide octahedral molecular sieve nanomaterials. *Adv. Funct. Mater.* **2006**, *16*, 1247−1253.
(43) Rani, B.; Ravi, G.; Yuvakkumar, R.; Hong, S. I.; Velauthapillai, D.; Thambidurai, M.; Dang, C.; Saravanakumar, B. Neutral and alkaline chemical environment dependent synthesis of Mn_3O_4 for oxygen evolution reaction (OER). *Mater. Chem. Phys.* **2020**, *247*, No. 122864.
(44) Rani, B. J.; Nivedha, K.; Ravi, G.; Yuvakkumar, R. Electrochemical Water Oxidation of $NiCo_2O_4$ and $CoNi_2S_4$ Nanospheres Supported on Ni Foam Substrate. *ChemistrySelect* **2019**, *4*, 10122−10132.
(45) Rani, B. J.; Praveenkumar, M.; Ravichandran, S.; Ganesh, V.; Guduru, R. K.; Ravi, G.; Yuvakkumar, R. Ultrafine M-doped TiO_2 (M= Fe, Ce, La) nanosphere photoanodes for photoelectrochemical water-splitting applications. *Mater. Charact.* **2019**, *152*, 188−203.
(46) Zhou, H.; Wang, Y.; He, R.; Yu, F.; Sun, J.; Wang, F.; Lan, Y.; Ren, Z.; Chen, S. One-step synthesis of self-supported porous $NiSe_2$/Ni hybrid foam: an efficient 3D electrode for hydrogen evolution reaction. *Nano Energy* **2016**, *20*, 29−36.
(47) Zhou, W.; Lu, J.; Zhou, K.; Yang, L.; Ke, Y.; Tang, Z.; Chen, S. $CoSe_2$ nanoparticles embedded defective carbon nanotubes derived from MOFs as efficient electrocatalyst for hydrogen evolution reaction. *Nano Energy* **2016**, *28*, 143−150.
(48) Yang, Y.; Zhang, W.; Xiao, Y.; Shi, Z.; Cao, X.; Tang, Y.; Gao, Q. $CoNiSe_2$ heteronanorods decorated with layered-double-hydroxides for efficient hydrogen evolution. *Appl. Catal., B* **2019**, *242*, 132−139.
(49) Achour, A.; Ducros, J. B.; Porto, R. L.; Boujtita, M.; Gautron, E.; Le Brizoual, L.; Djouadi, M. A.; Brousse, T. Hierarchical nanocomposite electrodes based on titanium nitride and carbon nanotubes for micro-supercapacitors. *Nano Energy* **2014**, *7*, 104−113.
(50) Mani, S.; Ramaraj, S.; Chen, S.-M.; Dinesh, B.; Chen, T. W. Two-dimensional metal chalcogenides analogous $NiSe_2$ nanosheets and its efficient electrocatalytic performance towards glucose sensing. *J. Colloid Interface Sci.* **2017**, *507*, 378−385.
(51) Zheng, Y.-R.; Gao, M.-R.; Gao, Q.; Li, H.-H.; Xu, J.; Wu, Z.-Y.; Yu, S.-H. An efficient $CeO_2/CoSe_2$ nanobelt composite for electrochemical water oxidation. *Small* **2015**, *11*, 182−188.
(52) Martins, C. A.; Fernández, P. S.; Troiani, H. E.; Martins, M. E.; Arenillas, A.; Camara, G. A. Agglomeration and cleaning of carbon supported palladium nanoparticles in electrochemical environment. *Electrocatalysis* **2014**, *5*, 204−212.

https://dx.doi.org/10.1021/acsomega.0c01476
ACS Omega 2020, 5, 14702−14710

(53) Kwak, I. H.; Im, H. S.; Jang, D. M.; Kim, Y. W.; Park, K.; Lim, Y. R.; Cha, E. H.; Park, J. $CoSe_2$ and $NiSe_2$ nanocrystals as superior bifunctional catalysts for electrochemical and photoelectrochemical water splitting. *ACS Appl. Mater. Interfaces* **2016**, *8*, 5327−5334.
(54) Chen, T.; Tan, Y. Hierarchical $CoNiSe_2$ nano-architecture as a high-performance electrocatalyst for water splitting. *Nano Res.* **2018**, *11*, 1331−1344.
(55) Liu, Y.; Cheng, H.; Lyu, M.; Fan, S.; Liu, Q.; Zhang, W.; Zhi, Y.; Wang, C.; Xiao, C.; Wei, S.; Ye, B.; Xie, Y. Low overpotential in vacancy-rich ultrathin $CoSe_2$ nanosheets for water oxidation. *J. Am. Chem. Soc.* **2014**, *136*, 15670−15675.
(56) Tang, C.; Cheng, N.; Pu, Z.; Xing, W.; Sun, X. NiSe nanowire film supported on nickel foam: an efficient and stable 3D bifunctional electrode for full water splitting. *Angew. Chem., Int. Ed.* **2015**, *54*, 9351−9355.
(57) Gerken, J. B.; McAlpin, J. G.; Chen, J. Y. C.; Rigsby, M. L.; Casey, W. H.; Britt, R. D.; Stahl, S. S. Electrochemical water oxidation with cobalt-based electrocatalysts from pH 0−14: the thermodynamic basis for catalyst structure, stability, and activity. *J. Am. Chem. Soc.* **2011**, *133*, 14431−14442.

https://dx.doi.org/10.1021/acsomega.0c01476
ACS Omega 2020, 5, 14702−14710